Susceptibility Assessment of Rainfall Induced Landslides: A Case Study of the Debris Flow on July 27, 2011 at Umyeonsan (Mt.), Seoul, Korea

Évaluation de la susceptibilité des glissements de terrain provoqués par les précipitations : une étude de cas de la lave torrentielle du 27 juillet 2011 à Umyeonsan (Mt.), Séoul, Corée

Chan-Young Yune
Department of Civil Engineering, Gangneung-Wonju National University, Korea

Sangseom Jeong
Department of Civil, Environmental Engineering, Yonsei University, Korea

Myoung Mo Kim
Department of Civil, Environmental Engineering, Seoul National University, Korea, geotech@snu.ac.kr

ABSTRACT: In Korea-70% of which is covered by mountains-landslides and debris flow hazards are frequently occurring in summer. Most of these hazards have been concentrated around mountainous region. On July 27, 2011, however, a total of 33 debris flows occurred in Umyeonsan (Mt.), around where is densely populated residential areas in Seoul, Korea. The debris flow hazard resulted in 16 fatalities and extensive damage to houses, roads, and other properties. Most of the debris flows were initiated from shallow landslides which were triggered by an intensive rainstorm with a peak intensity of 112.5 mm/h. This paper provides a comprehensive description of the debris flow hazards in Umyeonsan with the morphological, hydrological, and geotechnical features of the watershed. Also, GIS-based prediction methods of landslide susceptibility are highlighted. Based on this, countermeasures by combining elements of engineering solution such as ecological planting, stone channels, soil nailing, and concrete barriers, have been designed and constructed.

RÉSUMÉ : En Corée - dont 70% est couvert par des montagnes - des glissements de terrain et des risques de lave torrentielle se produisent fréquemment en été. La plupart de ces dangers ont été concentrés autour de la région montagneuse. Le 27 juillet 2011, cependant, un total de 33 lave torrentielles s'est produit à Umyeonsan (Mt.), autour d'où se trouvent des zones résidentielles densément peuplées à Séoul, en Corée. Le risque dû à l'écoulements de débris a entraîné 16 morts et des dommages importants aux maisons, aux routes et à d'autres propriétés. La plupart des écoulements de débris ont été provoqués à partir de glissements de terrain peu profonds, déclenchés par une tempête violente avec une intensité maximale de 112,5 mm / h. Cet article fournit une description complète des dangers du ruissellement des débris à Umyeonsan avec les caractéristiques morphologiques, hydrologiques et géotechniques du bassin hydrographique. De plus, les méthodes de prévision basées sur le SIG de la susceptibilité aux glissements de terrain sont mises en évidence. Sur cette base, des contre-mesures ont été conçues et construites en combinant des éléments de la solution d'ingénierie tels que la plantation écologique, les canaux en pierre, le clouage des sols et les barrières de béton.

KEYWORDS: landslide, debris flow, Umyeonsan, landslide susceptibility, intensive rainstorm

1 INTRODUCTION

Debris flows are a mass movement process in mountainous terrain. The term debris flow is defined as a very rapid to extremely rapid surging flow of saturated debris in a steep channel that involves a high degree of entrainment of material and water along the flow path (Hungr et al. 2013). Debris flows differ from other types of landslides because they move rapidly, travel long distances, increase in volume by entrainment, and are difficult to predict. The activiey of a debris flow depends on the hydrology, lithology, topography, vegetation, and drainage conditions, which contribute to the magnitude, frequency, initiation mechanism, and morphology of a debris flow (Innes 1983, Coussot and Meunier 1996). During a debris flow event, channels with thick unconsolidated soils are often eroded and supply large quantities of poorly sorted debris. The relationship between rainfall and debris flow initiation, however, is not simple and depends on factors such as the rainfall pattern, antecedent moisture content, and topographic relief (Deganutti et al. 2000; Zhou et al. 2014).

The occurrence of debris flows in weak heterogeneous deposits such as colluvium has been previously observed in East Asia (Chen 1987; Fuchu et al. 1999) and North America (Fleming et al. 1989, Coe et al. 2008) because these regions experience intense rainfall. In Korea, 70% of which is covered by mountains, landslides and debris flow hazards frequently occur in the summer. Additionally, the frequency and the amount of rainfall associated with seasonal rain and typhoons are increasing, and debris flows triggered by rainfall have increased as well. On July 27, 2011, 33 debris flows and 151 landslides were triggered by an extreme rainfall event in Umyeonsan (Mt.), Seoul, Korea. After the occurrence of the slope hazard, a field and laboratory investigation was conducted to explore the causes and mechanisms of the debris flows, and several reports and papers were presented (KGS 2011; Yune et al. 2013; SI 2014; Kim et al. 2014a; Jeong et al. 2015).

This paper provides a comprehensive description of the landslide and debris flow hazards in the Umyeonsan area, around which are the densely populated residential areas of Seoul, Korea, with the morphological, hydrological, and geotechnical features of the watershed. Also, GIS-based prediction methods for landslide susceptibility are introduced. Becuase the authors took part in the investigation on several occasions, the investigation results in the investigation reports are included as well.

2 OVERVIEW OF 2011 DEBRIS FLOW AT UMYEONSAN

2 .1 *General features of Umyeonsan (Mt.)*

Umyeonsan(Mt.) is located southeast of the metropolitan city of

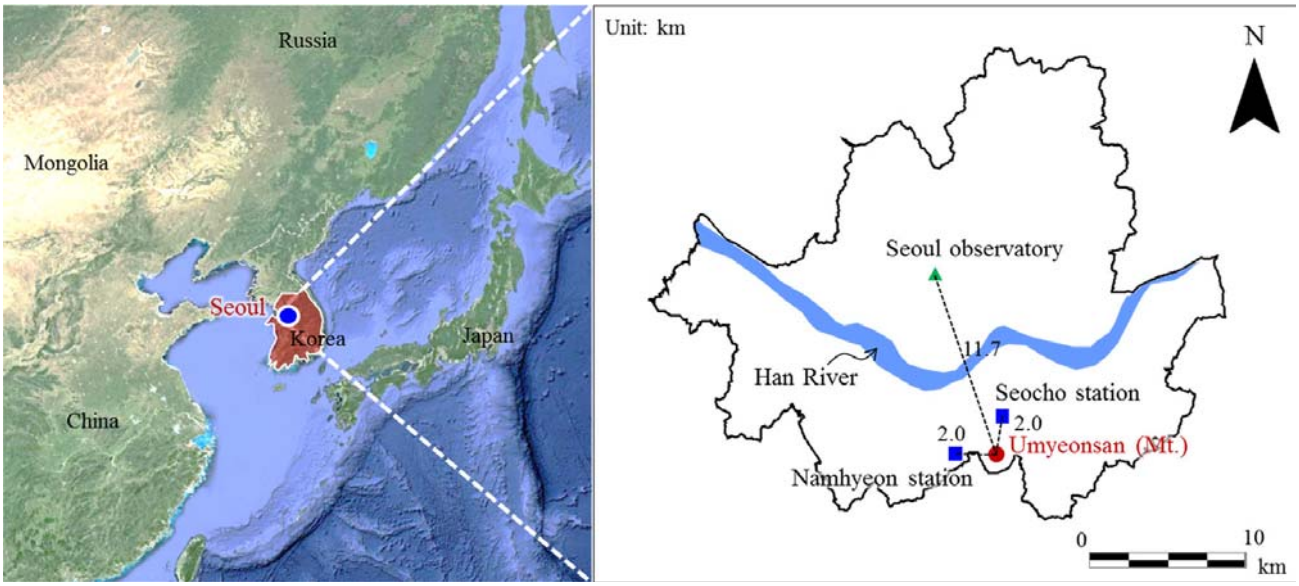

Figure 1. Locations of the Umyeonsan and near weather stations (Jeong et al. 2015)

Seoul, Korea shown in Figure 1. The topography is characterized by steep hills, gullies, and valleys (slopes are normally less than 40°) with elevations ranging from approximately 50 to 312.6 m above sea level. The area is underlain by metamorphic Precambrian gneissic rocks that belong to the Gyeonggi massif. The bedrock is primarily composed of quartz, plagioclase, biotite, amphibole, and feldspar. Some folds and foliations seem to cause relative displacements in the rock. The bedrock is heavily fractured, intensely weathered, and covered by a layer of colluvium. The vegetation cover is dense and comprises coniferous and deciduous forests, mixed forests of soft and hardwood, and understory vegetation.

The Umyeonsan region is situated in the temperate monsoon zone. Thus, the area is generally hot and humid with abundant rainfall in summer and cold and dry in winter. The average annual precipitation ranges from 1100 to 1500 mm with 70 % of the annual average falling from June to September. In the area, small landslides and debris flows commonly occur during the summer season, although the July 27, 2011 disaster has been the most catastrophic of all the recorded debris flows. The intensity of this event is, to some extent, attributable to the climate change, in terms of the higher intensity and longer duration of rainfall not only in the Umyeonsan region but also in most regions in Korea (Kim et al. 2012; Le and Bae 2013).

2 .2 *Landslide and debris flow hazard*

In 2010, regional intensive rainfall following Typhoon Kompasu caused a few slope failures in Umyeonsan (Mt.), and two of them developed as debris flows at the northern gullies. The Seoul Metropolitan Government started rehabilitation work for the damaged watersheds; however, the damage in 2010 was not significant compared to the debris flow hazard in 2011.

In the following year, between 7:40 and 8:50 a.m. on July 27, 2011, many landslides and debris flows occurred simultaneously all around Umyeonsan (Mt.) including two watersheds where there had been a previous debris flow event in 2010. Because the mountain is located at the center of a dense residential area, the hazard had a great impact on the society compared to debris flows that have occurred in rural areas, and it led to a careful scrutiny of the causes of debris flows for the hazard area. Buildings were damaged by flooding and also partly or completely destroyed as summarized in Table 1. In total, 16 people were killed around the Umyeonsan area. Even though the number of complete and partial destruction of buildings listed in Table 1 was 1 and 10, respectively, there were more than 20 unauthorized shacks destroyed on the western side of Umyeonsan (Jeonwon watershed in Table 2) which were not officially recorded in the damage statistics (Figure 2).

Figure 2. Destructed shacks in western side of Umyeonsan (Jeonwon watershed)

Table 1. Damages around Umyeonsan (Mt.) on 27 July 2011.

Flooding		Destruction of buildings		Fatalities
House	Shop	Complete	Partial	
2,103	1,584	1	10	16

Right after the hazard, an aerial photo was taken. Figure 3 shows photos taken before and after the hazard. Many research teams were involved in the investigation of the hazard. However, only two investigations were officially conducted by the Seoul Metropolitan Government (KGS 2011; SI 2014). In November 2011, the Korean Geotechnical Society (KGS 2011) produced an official report on the causes of the landslides and on the restoration of the site. The report, however, only included results for 4 watersheds heavily damaged by the landslides and debris flows. The report outlined the geology and the mechanism of the landslide and debris flow, and briefly described the measures to be taken to restore the respective watershed. When the report was released, the bereaved families and the residents who suffered property damages by the hazard vigorously protested against the report. Moreover, various civic

(a) Aerial photo taken before debris flow hazard

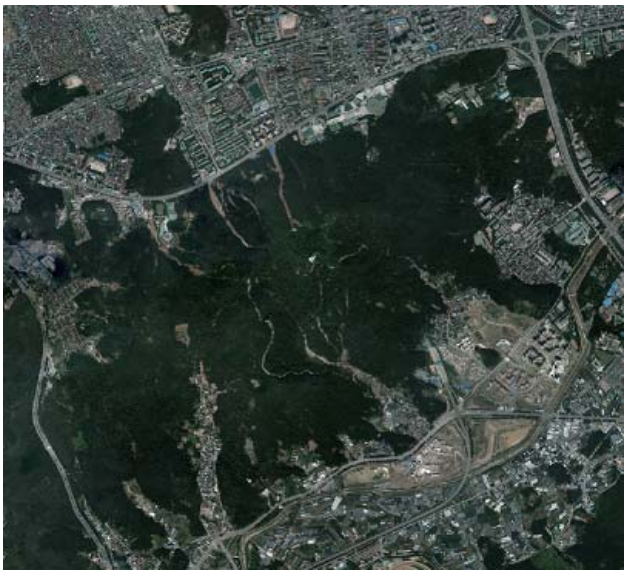

(b) Aerial photo taken after debris flow hazard

Figure 3. Aerial photos of the Umyeonsan in (a) 2009 and (b) 2011 (SI 2014).

groups supported the protests. Their dissatisfaction came from the fact that the causes of the landslides were studied mechanically only from an academic standpoint. Because of these demands from the residents and civic groups the Seoul Metropolitan Government launched a second investigation in 2012 for the whole area of Umyeonsan, and the report was released in 2014 (SI 2014). The authors were involved in the second official investigation and other previous investigations.

2 .3 *Rainfall conditions*

There are 2 automatic weather stations close to Umyeonsan (Mt.) as shown in Figure 1. Figures 4 (a) and (b) show the hourly and cumulative rainfall from July 26 to 27, 2011 recorded at the Namhyun and Seocho stations. The cumulative rainfall for 24 hours at 4:00 p.m. on July 27, 2011 right after the end of the rain at the Namhyun and Seocho stations after the debris flow hazard was 425.5 and 364.5 mm, respectively. The maximum hourly rainfall at the two stations was 112.5 and 85.5 mm, respectively, and occurred between 7:40 and 8:40 a.m. on July 27, 2011. The most severe maximum 1-h rainfall was recorded at the Namhyun station with a corresponding return period longer than 120 years. Interestingly, the time of peak hourly rainfall coincided well with the time of the debris flow occurrence in the Raemian watershed (on the northern slope of Umyeonsan which started at 8:30 a.m.). The elevations of the two stations are 87.1 and 35.5 m a.s.l., respectively, which are lower than those of the debris flow initiation areas (approximately 260 m a.s.l.). Taking into account the orographic effect (i.e., rainfall normally increases with elevation), the amount and intensity of the rainfall that fell on the actual debris flow initiation areas might be higher than the values recorded at the two stations. Figure 5 shows the wind direction and velocity for the period from July 25 to July 27, 2011 at the Namhyeon and Seocho stations. The major wind directions were ENE and SSW for the Seocho and Namhyeon stations, respectively. Consequently, the wind observed at the other side of the mountain blew toward Umyeonsan and might have poured excessive rainfall at the summit of the mountain.

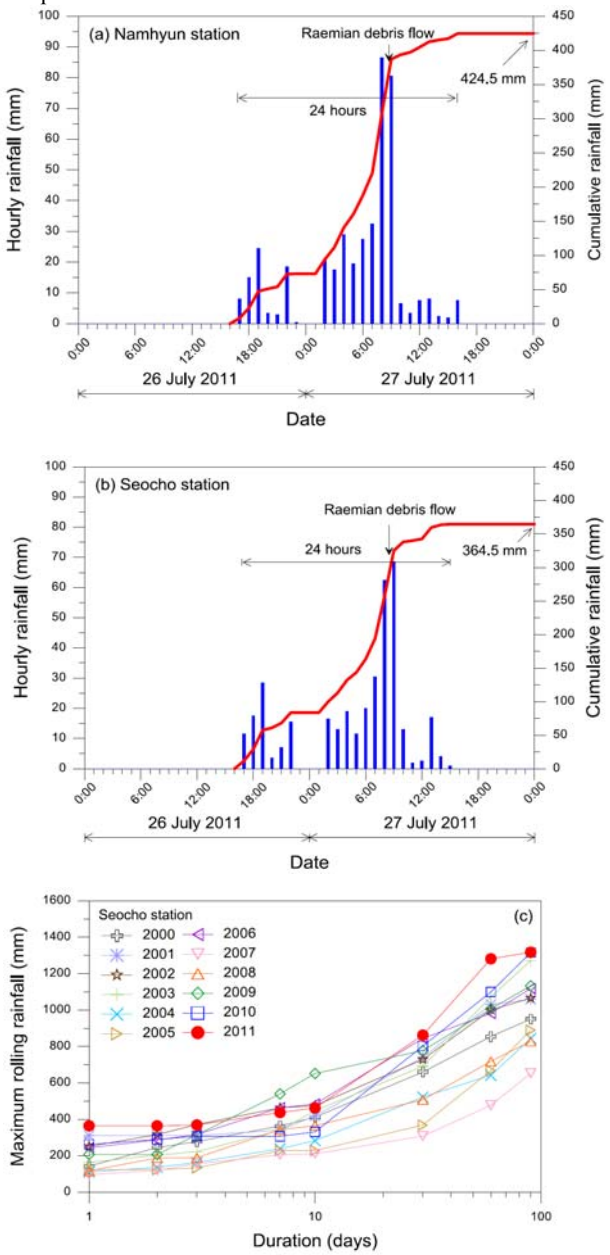

Figure 4. Hourly and cumulative rainfall for 26–27 July 2011 and maximum rolling rainfall quantities recorded at Seocho station (Jeong et al. 2015)

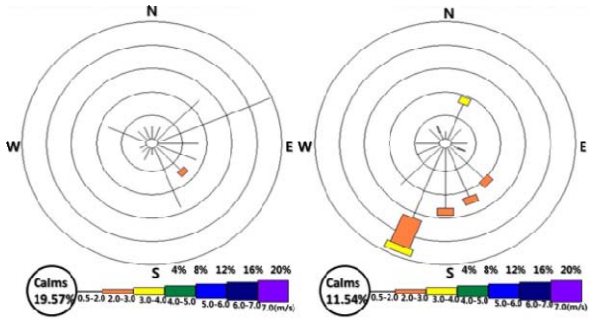

Figure 5. Wind rose of Namhyeon and Seocho stations from 25th July to 27th July 2011 (Yune et al. 2013)

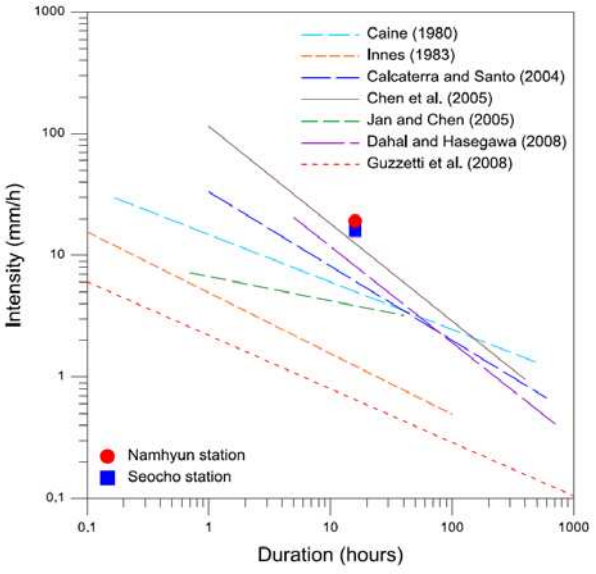

Figure 6. Hourly and cumulative rainfall for 26–27 July 2011 and maximum rolling rainfall quantities recorded at Seocho station (Jeong et al. 2015)

Furthermore, for the 2011 rainstorm, the heaviest continuous rainfall was recorded as longer than 10 days. Because a rain gauge at the Namhyeon station was installed in 2010, the rainfall data from the Seocho station, where the recording started from January 2000, was used for the long term effect of rain. The maximum rolling rainfall and duration at the Seocho station were plotted in Figure 4 (c) for 12 years. The long-duration cumulative rainfall longer than 30 days (1 to 3 months) was the highest compared to those of the previous rainstorms in the Umyeonsan area since January 2000. The cumulative rainfall for 2 and 3 months before the debris flow event was 1,281.5 and 1,317.5 mm, respectively. Those values were comparable to the average annual rainfall in Seoul. Based on the rainfall analyses, the high intensity of the rainfall in the short-term and long-term had a critical role in the development of the debris flows.

Rainfall intensity-duration (ID) thresholds are commonly used to predict the temporal occurrence of debris flows. These thresholds represent the lower limit of peak rainfall intensities that induce debris flows. Empirical ID thresholds are usually in the form of the following equation (Guzzetti et al. 2008):

$$I = \alpha D^{\beta} \quad (1)$$

,where I is the rainfall intensity (mm/h), D is the duration (hour), and α and β are empirical constants. Considering the duration of the rainfall (16 h) prior to the debris flow at the Raemian watershed (Table 2) and the corresponding cumulative rainfall of 306.5 mm at the Namhyun station, the average rainfall intensity is 19.2 mm/h. For the Seocho station, the average rainfall intensity for the same time period is 16.0 mm/h. In Figure 6, the recorded rainfall of this rainstorm was higher than the ID thresholds proposed by many researchers. These results suggest that the intense rainfall caused higher moisture conditions and an increase in pore water pressure in the colluvium, resulting in the debris flow events.

3 SITE INVESTIGATION

A comprehensive field and laboratory study was carried out to investigate the spatial distribution and geomorphological features of the debris flows and to determine the hydrogeological, geotechnical, and vegetation characteristics of the hazard area. This investigation included visual inspection, interpretation of aerial photographs, construction of a digital elevation model (DEM), analysis of rainfall records, in situ and laboratory tests, and a plant community survey.

3 .1 *Field survey*

3.1.1 *Landslides and debris flows*

The field survey was conducted right after the debris flow hazard. Aerial photography was also used to confirm the locations and characteristics of the debris flows. The combination of 1:5000-scale topographic maps and global positioning system (GPS) data was used to establish the topography of the debris flows. Geodetic data were used to construct a digital elevation model (DEM) with an accuracy of 1 m in elevation, and the DEM was then analyzed to obtain morphological information on the debris flow watersheds. Even with the aid of the aerial photographs and topographic maps with DEM, however, it was difficult to determine the detailed flow path and all initiation locations because of the thick forest as shown in Figure 3 (b). Thus, the field investigation was essential to provide detailed debris flow gullies and the locations of landslides which were the initiation points of the most of the debris flows. During the field investigation, the channel width, gradient, and direction were recorded for every 20 m length following the flow path to the initiation point. The size and volume of the initiation landslides were estimated, and the gradient of the initiation locations was measured by the field investigation as well.

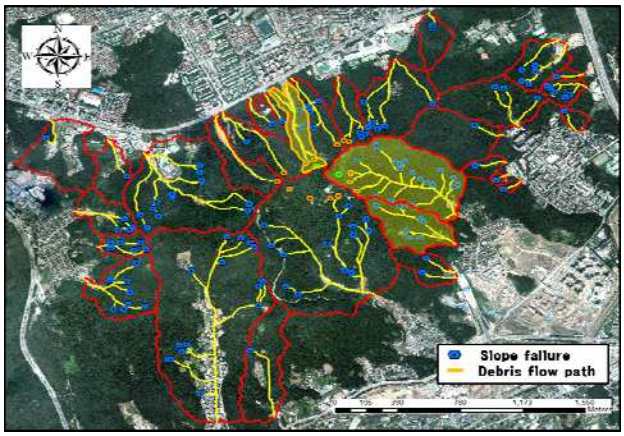

Figure 7. Result of field investigation on the 33 debris flow gullies (marked in yellow lines) and 151 landslides (i.e., debris flow initiation points denoted by blue and orange circles) in the 30 watersheds (outlined by red lines) (SI 2014).

Table 2. Morphological characteristics of the 33 debris flows in the 30 watersheds (Data from SI 2014)

Flow direction	Watershed	Number of debris flows	Basin area (x 10^3 m^2)	Average channel gradient (°)	Runout distance (m)	Landslides (initiation area)		
						Number	Average volume (m^3)	Average slope (°)
North	Daeseongsa	1	57.0	15.9	130.6	2	8.1	37
	Arthall	2	183.6	19.4	562.9	8	112.3	40
	Gugakwon	1	76.2	20.9	495.2	5	86.9	35
	Deokuam	1	90.8	20.1	625.3	5	98.7	35
	Raemian	1	75.6	19.0	606.7	4	1827.0	44
	Limkwang1, 2	2	54.1	16.2	267.3	2	45.7	29
	Shindonga1, 2	2	214.4	17.5	663.6	3	105.0	26
	Bodeoksa	1	421.4	17.8	900.0	12	153.6	36
	Apwit1, 2	2	233.4	12.0	307.1	2	19.8	16
West	Jeonwon1, 2, 3	3	271.8	15.6	454.4	22	62.9	27
South	Dwitgol	2	786.4	15.8	1365.1	15	34.2	35
	Angol	1	178.2	15.0	632.0	1	125.2	26
	Songdong	1	678.9	19.7	941.3	18	182.0	36
	U. tunnel	1	64.2	17.6	229.7	2	129.3	29
	Hyeongchon1, 2	2	444.8	21.7	960.3	31	75.4	34
	EBS1, 2, 3	3	41.4	16.9	201.5	3	70.2	29
	Gwanmunsa1, 2	2	324.0	17.6	385.4	4	73.2	30
	Amsan	1	17.7	15.0	176.3	1	108.6	33
East	Gangnam1, 2	2	48.9	15.6	246.8	6	55.4	34
	Yangjae	2	90.9	13.3	435.7	5	134.3	40
Total		33	4353.7	-	10,450.2	151	3507.8	-

Figure 8. Photographs taken at the initiation, transportation, and deposition areas of debris flows: (a) main scarp of a shallow transitional slide at a ridge crest, (b) erosion of colluvium in the center of a channel, (c) expose of the gneiss bedrock, and (d) debris flow material consisting of soil, rocks, and woody debris (KGS 2011)

The result of field investigation with the aid of DEM is shown in Figure 7 and Table 2. Figure 7 shows the 33 debris flows and 151 landslides that occurred in 30 watersheds in the Umyeonsan area. In Table 2, the name of each watershed is listed from the top northeast catchment in Figure 7 in a counterclockwise direction. As shown in Figure 7 and Table 2, when the initiation and moving direction of the debris flows were classified by direction, it was found that many of the slope failures and debris flows occurred on the northern and southern slopes. Most of the landslides are concentrated along the ridgeline of the mountain due to the high slope angle. The slope material has a low density and low strength. Debris flows with different origins and features are observed, and certain flows have been incised by gullies.

Most of the debris flows moving towards the south were channelized debris flows which flowed down along the gully and merged together. On the other hand, many debris flows on the northern slope were hillslope debris flows which moved rapidly without being confined in an established channel. The surface areas of the watersheds range from 17,700 to 786,400 m^2, with an average of 217,685 m^2, and approximately half of the watersheds are smaller than 105 m^2. The channel gradient and runout distance of the debris flows are less than 21.7° and 1365.1 m, respectively. Individual watersheds contain 1 to 31 landslides, which served as the primary source of the material for the initiation of the debris flows. The volumes of the initiation landslides range from 8.1 to 1,827.0 m^3. In particular, the Raemian watershed has the largest initial volume, with a value of 1,827 m3, which represents 52 % of the total landslide volume. The slope angle of the initiation landslides varies from 16 to 44°. Importantly, 60 % of the landslides occurred on slopes steeper than 30°, indicating that the debris flows preferentially initiated on slopes steeper than 30°. These survey results are supported by previous investigations on the other debris flow sites (Fuchu et al. 1999; Tiranti et al. 2008; Yune et al. 2011).

The field survey revealed that the debris flows in the Umyeonsan area started from the vicinity of the crest as a shallow landslide of the loose colluvium overlying the gneiss bedrock (Figure 8 (a)). In most of the transportation areas, the front surge and the main body of the debris flows eroded gullies evenly at about a 1 to 1.5 m depth, and the total volume increased by more than 10 times. After that, hyperconcentrated flows with higher water content followed and eroded the colluvial layer forming narrow creeks reaching the bedrock at around a 1 to 2 m depth (Figure 8 (b)). The gneiss bedrock, which is deeply fractured and highly weathered, was commonly exposed (Figure 8(c)). In general, gneiss has thick weathering layers enriched in fine particles and clay minerals. The transported debris was deposited at the confluence of the gullies and the toe of the mountain. The debris flows typically comprised soil and rocks of various sizes and shapes and variously graded deposits as well as woody blocks and man-made materials (Figure 8(d)).

Raemian watershed

The most catastrophic debris flow occurred in the Raemian watershed (shaded area on the northern slope in Figure 7). In the debris flow initiation area, four discrete landslides occurred with an average volume of 1827 m^3. It was the largest landslide volume compared to other initiation landslides with the average volume ranging from 19.8 to 182.0 m^3 shown in Table 2. Figure 11 (a) and (b) shows two initiation landslides at the top of the watershed. Those two landslides induced debris flows that merged into a single flow due to the local topography right below the initiation locations, and two more landslides joined in the middle part of the flowing path. The initial volume in the two landslides was approximately 4,000 m^3; however, the total volume of the debris flows deposited in the downstream road

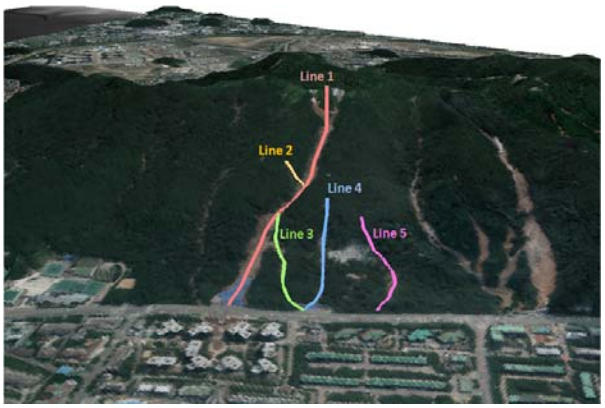

(a) Raemian watershed

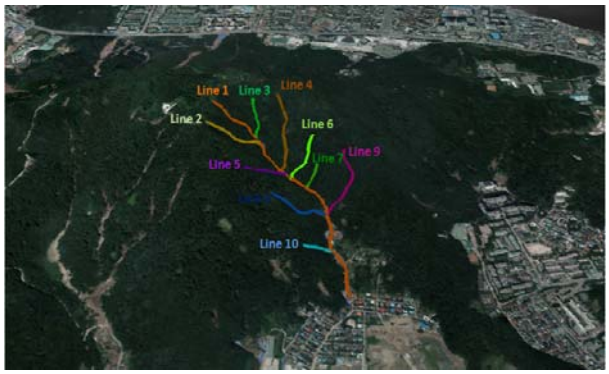

(b) Hyoungchon2 watershed

Figure 9. Debris flow path in 3 dimensional photo after hazard (SI 2014)

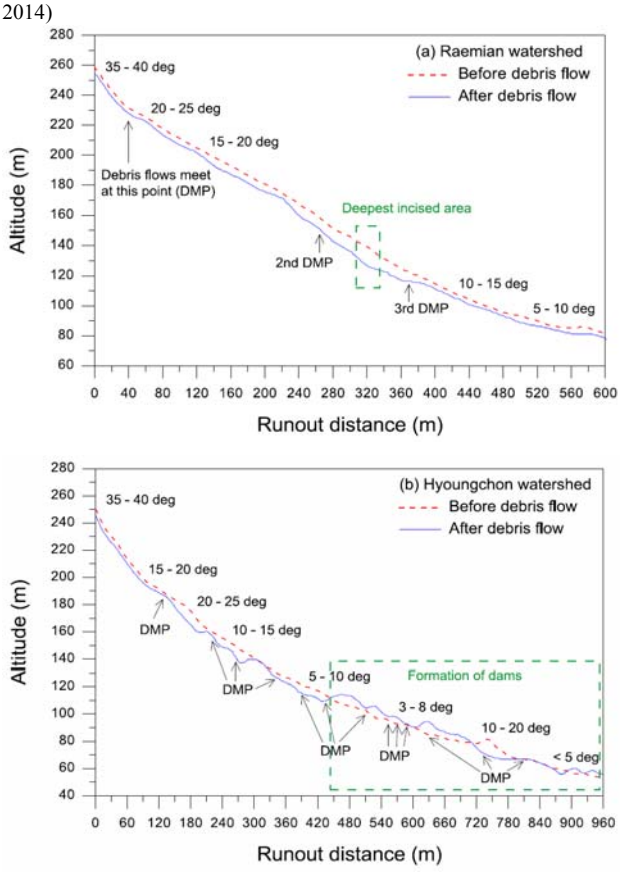

Figure 10. Longitudinal profile of the debris flow gullies in (a) Raemian and (b) Hyoungchon2 watersheds. (Note that the elevation difference between the before and after of the debris flow occurrence is exaggerated by a factor of 3.) (SI 2014)

Figure 11. Initiation landslides in Raemian ((a) and (b)) and Hyongchon ((c) to (f)) watersheds.

and built-up areas was about 32,000 m3. Grain size distribution analyses have been carried out on material sampled in the initiation, transportation and deposition areas. The mean diameter of the materials was about 1 mm, while the mean percentage of the fine materials (finer than 0.065 mm) is about 35% (Yune et al. 2013).

The longitudinal profile along the debris flow path follows line 1 in Figure 9 (a) featuring a channel length of 632 m, a width of 30 to 40 m, and an average incised depth of 1.6 m (Figure 10 (a)). The upslope elevation of the gully is 260 m a.s.l and the gully mouth is at 80 m a.s.l. The deepest incised depth is 4 m, which is located at an elevation of approximately 120 m asl and at a runout distance of 320 m. As the elevation of the gully decreases, the gradient gradually decreases from 40 to 5°.

In the field survey, groundwater was observed seeping out of the bedrock underlying the sliding mass at the initiation area. This seepage could have generated an upward force and high pore water pressure in the slip zone. Additionally, a several-centimeter-thick layer of clayey soil was observed between the colluvium and the gneiss bedrock. The overlying colluvium may have acted as a highly permeable material that led to the formation of a perched water table. The permeability contrast between the clay and colluvium could have produced a high pore water pressure, which facilitated the sliding process. The debris flow crossed the road and rushed into the Raemian apartment, killing three people and damaging houses, vehicles, and the water sewage system. Additionally, material was deposited on the road and in the residential area. The deposited material was a poorly sorted, matrix-supported mixture of angular rock fragments and fine-grained soils. Relatively large boulders and woody debris were found in the uppermost part of the deposit.

Hyongchon watershed

The debris flow event in the village of Hyoungchon involved debris flows in two watersheds separated by a ridge (shaded area on the southern slope in Figure 7). Here, the features of the Hyongchon2 watershed is discussed, which has a larger area and contains 23 landslides. It has the largest number of initiation landslides; however, the volume was relatively small with an average of 75.4 m^3. Most of the initial landslides in the Hyongchon2 watershed were shallow landslides on a small scale with a 0.3 to 1 m depth as shown in Figure 11 (c) to (f).

The longitudinal profile along the debris flow path follows line 1 in Figure 9 (b), which features a channel length of 980 m, a width of 10 to 15 m, and an average erosion depth of 1.5 m (Figure 10 (b)). The upslope elevation of the gully is 250 m a.s.l., and the gully mouth is at 55 m a.s.l. The gradient of the gully is the highest at the crest of the valley slope (35–40°) and decreases further down the slope (<5°). The deepest erosion depth, 3.5 m, is present at a runout distance of 180 m. After a runout distance of approximately 460 m, the debris materials start to deposit as the channel gradient becomes gentle and the channel width starts to enlarge to 20 m.

One unique feature different from the other watersheds is that there was an ecological park with a reservoir at the end of the watershed (location of the embankment is at 740 m shown in Figure 10 (b)). The reservoir has an area of 2,430 m^2 with 1 to 1.5 m depth. At the debris flow event, it acted as a deposition area with a check dam (Figure 12 (b)). Therefore, it could contain a significant amount of debris inside of it and could reduce the damage in the downstream area. The embankment, however, was damaged by overflowing water because the spillway at the corner of the embankment was blocked by woody debris. The overflow eroded the embankment, and the width and depth of the eroded part were 19 and 8 m, respectively (Figure 12 (a)). Consequently, a flash flood inundated the Hyoungchon village, killing one person and destroying local infrastructures.

Figure 12. Photos viewing upstream on (a) collapsed embankment and (b) deposited debris inside the reservoir of the ecological park in Hyongchon2 watershed.

3.1.2 *Velocity*

One of the most interesting features of the debris flow in Umyeonsan (Mt.) is that video clips were recorded by residential people and by the blackbox of a vehicle passing by. They are the first videos of a real debris flow captured in Korea (http://www.youtube.com/watch?v=J2vkhY7gqQM and http://www.youtube.com/watch?v=L0ctCSZIHto). In general, the velocity of a debris flow is backcalculated from the observed superelevation of the flow which requires a subjective estimation of the channel's radius of curvature. It can also be predicted by solving flow equations that use appropriate rheological models and material property inputs (Prochaska et al. 2008). The most accurate method for estimating the debris flow velocity is to directly estimate it from a real debris flow in the field. Two videos were recorded by residential people in the Raemian watershed, and one video was recorded by the blackbox of a passing vehicle near the Shindonga2 watershed. Figure 13 shows photos taken during the site survey, and still images captured from the videos.

The velocities of the debris flows were estimated based on the moving distance measured in the field and the number of frames containing the movement of the front surge of the debris flows crossing certain distances. The estimated results revealed that the maximum velocities of the front surge of the debris flows in the Raemian and Shindonga2 watersheds were 28.6 and 18.3 m/s, respectively. A field observation by Son et al. (2012) showed that the groundwater level at locations where the debris flows initiated reaches the surface such that surface runoff occurs during a continuous rainfall condition of more than 250 mm, even if there is no significant antecedent rainfall. As observed by Iverson et al. (2011), surface runoff at the slope

Figure 13. Photos and still images from videos at downstreams of (a) Raemian and (b) Shindonga2 watersheds.

can decrease the sediment volume concentration and increase the propagation speed.

Although the Raemian and Shindonga2 watersheds are not far apart and have similar mean watershed slopes, the debris flows, which simultaneously occurred at both watersheds, had a significant difference between their velocities. The relatively slow velocity of the debris flow at Shindonga2 was due to a contraction of the channel width right before the meeting point of the channel and the road and a slight change in the flow direction just upstream of the road.

3.1.3 *Geology*

The tectonic province of the Umyeonsan (Mt.) area is the Gyeonggi massif which consists of Precambrian gneisses and schists intruded by Mesozoic granitoids. Umyeonsan (Mt.) is located near the southern tip of the Dongducheon Fault with NNE-trending and adjacent to a NE-trending fault. In the Umyeonsan(Mt.) area, ENE-WSW striking faults are the most dominant, and faults oriented in the NW-SE direction are also found frequently based on the results of lineaments extraction from high resolution (1 m) IKONOS images (Figure 14). To correct for the geometric distortion caused by the topographic relief, orthorectification was performed before the extraction of the lineaments. The lineaments extracted from the Landsat images, digital elevation map (DEM) and aerial photographs also showed similar strikes. The density of the lineaments is higher in the Hyeongchon, Dwitgol, Jeonwon and Shindonga watersheds which were more damaged in the 2011 debris flow.

Umyeonsan (Mt.) is composed of highly-weathered banded gneiss with subordinate granitic gneiss and granite. The bedrock is primarily composed of quartz, plagioclase, biotite, amphibole, and feldspar. The bedrock is heavily fractured, highly weathered, and covered by a layer of colluvium with varying thicknesses from a few centimeters to 13 m especially in the northern slope. The boundary between the base rocks and colluvium deposits usually is filled with a thin clay layer several cm in thickness and consisting of illite and kaolin. The colluvial deposit consists of a poorly sorted mixture of sands and gravels in a silty matrix. The banded gneiss is well-foliated with a preferred alignment of biotite in the mafic band. Locally, the felsic band (quartz and feldspar) of the banded gneiss is too thin and the banded gneiss appears almost as a schist. The granitic gneiss is usually weakly-foliated. The foliation of these gneisses dominantly strikes northeast.

3.1.4 *Forestry*

Umyeonsan (Mt.) is under a moderate monsoon climate. More than 80% of the entire forest is classified as a broadleaved forest in digital forest stock maps which were generated by the Korea Forest Research Institute. To explore the species distribution and diversity of the vegetation communities, a field survey was performed in the upper ridges of the Raemian and Deokuam watersheds. All living trees with a diameter at breast height (DBH) larger than 6 cm were counted in 6 circular areas with a radius of 11.3 m. A total of 149 wood species were investigated, and the characteristics of the vegetation communities, including species, DBH, height, and root depth, were recorded (Table 3). Twelve dominant woody species were identified in the Raemian watershed, and their characteristics are listed in Table 4.

The species composition is dominated by Quercus mongolica (43 %), known as the Mongolian Oak. Because the Mongolian Oak grows rapidly, it has been widely used in the region to prevent soil erosion and shallow landslides. Most forests in Umyeonsan (Mt.) are fully stocked with high canopy density, and the estimated distribution is 700~1,000 trees per hectare. However, vegetation species and coverage in herbaceous understory varies from watershed to watershed. In natural forests, the average height and DBH of most trees were estimated to be 20 m and 20 cm, respectively. These are not large enough values compared to their age of 40 years. In artificial forests, however, age and growth of trees vary depending on their species and planting year. The field survey also revealed that the root depths appear to be restricted to the surface layer of 1 m or less especially on the northern slope, although the majority of the colluvium thicknesses in debris flow areas are in the range of 1 to 2 m. In other words, most of the roots are located within a relatively shallow depth in the colluvial deposits while tap roots and deeply penetrating roots can be found on the southern slope of the Umyeonsan area. The roots in the shallow depth on the northern slope of Umyeonsan seems to prevent the runoff-induced erosion of the loose surface deposits to some extent and help to conserve the soil (Figure 15).

(a) Extraction of lineaments from high resolution IKONOS image

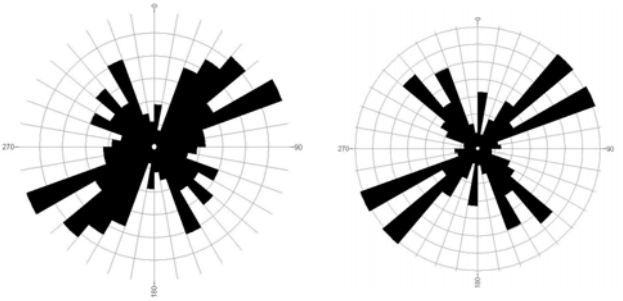

(b) Frequency rose diagram (c) Length rose diagram

Figure 14. Direction and frequency of lineaments extracted from IKONOS image (SI 2014).

Table 3. Species diversity of the vegetation communities in the upper ridges of Raemian and Deokuam watersheds (SI 2014)

Species	Number	Frequency (%)	DBH (cm)	Average height (m)
Quercus mongolica	64	43.0	23.1	10.7
Sorbus alnifolia	20	13.4	9.5	6.9
Acacia catechu	15	10.1	28.5	12.1
Pinus koraiensis	15	10.1	10.8	6.3
Pinus rigida	14	9.4	15.7	12.0
Prunus sargentii	9	6.0	11.7	6.3
Alnus japonica	4	2.7	21.0	10.5
Quercus dentate	3	2.0	15.0	8.7
Castanea crenata	2	1.3	21.5	10.5
Larix kaempferi	1	0.7	20.5	13.0
Betula davurica	1	0.7	21.0	10.0
Aesculus turbinate	1	0.7	22.0	9.0

Figure 15. Exposed roots in transportation area of debris flow in northern slope of Umyeonsan (Mt.).

3 .2 *Geotechnical investigations*

To scrutinize the detailed features of the debris flow hazard on July 27, 2011, geotechnical investigations were conducted in three watersheds (Raemian, Deokuam, and Hyongchon2). Seven boreholes were drilled to confirm the previously described stratigraphy and to perform *in situ* tests, such as the standard penetration test (SPT), constant head permeability test, and borehole shear test. Eight trial pits were also excavated to characterize the surficial materials that remained along the debris flow gullies, and disturbed and undisturbed soil samples were also obtained for laboratory tests. Laboratory tests to characterize the colluvial soil were conducted to determine (1) soil classification, (2) water content, (3) Atterberg limits, (4) grain size distribution, (5) soil-water characteristic curves, and (6) shear strength parameters. To determine the shear strength parameters, the direct shear test was performed under drained conditions, and the displacement rate of the direct shear test was 1 mm/min. All laboratory tests were performed in accordance with the procedures specified by the American Society of Testing Materials (ASTM).

The blow count of the standard penetration test (N value) in the colluvium layers is 4 to 5. In general, N values less than 10 indicate that the soil is very soft and loose (Bowles 1997). Therefore, the colluvial deposits are inferred to have provided the material in the debris flows. The N value of the weathered rock varies from 12 to 50/10 depending on the degree of weathering. Table 4 summarizes the results of the constant head permeability and shear tests in the boreholes. The permeability of the colluvium is approximately 10^{-6} m/s, and the permeability of the weathered rock is on the order of 10^{-7} m/s. The cohesion and friction angle of the colluvium layers at a 1 to 2 m depth were below 10 kPa and 26 °, respectively. Those strength parameters are relatively small and can be classified as soft ground which can be eroded easily and provide debris materials during a debris flow event.

Table 5 summarizes the physical properties of the soil samples obtained from depths of 0.15 to 0.5 m in the colluvium. The water contents ranges from 14.1 to 32.1 %, indicating that the surficial layer is wet and that the soils exhibit a high degree of saturation. The plastic and liquid limits of the soils are in the range of 20.9 to 23.8 % and 30.2 to 42.1 %, respectively. The proportions of fines (i.e., silty and clay) in the colluvial deposits are in the range of 28.8 to 55.7 %. Fines help sustain high pore water pressures in the debris flow thereby promoting travel distances (Iverson 2003). Iverson (2003) also reported that slurries with as little as 2 % of mud exhibit a debris flow activity and produce deposits with a characteristic debris flow morphology. The proportion and plasticity of the fines in the source material seem to have an important role in the development of the debris flows. According to the Unified Soil Classification System (USCS), the colluvial soils are classified as SM and SC-CL. The direct shear test of the undisturbed soil samples indicates that the average values for the cohesion and friction angle are 9.2 kPa and 24.8°, respectively, which are similar to those from the in situ borehole tests.

4 SUSCEPTIBILITY ASSESSMENT OF LANDSLIDES

4 .1 *Landslide analysis models*

Many empirical and analytical models have been proposed for susceptibility assessment of landslides. The YS-slope model has been developed to simulate the potential occurrences of shallow landslides on unsaturated soil by rainfall-infiltration, storage, recharge and groundwater flow processes (Kim et al. 2014b). This physically-based prediction model is based on a geographic information system (GIS) (Soller et.al; 1999), and data sets including topographic, soil depth, precipitation and geotechnical parameters were built to raster data with a matrix structure. Even though, the data structure of the YS-Slope model is based on the raster data of the GIS, it does not perform any data conversion excepting for setting up the initial data in contrast with previous methods using a hydrological model.

Table 4. In situ soil properties from constant head permeability test and shear tests performed in boreholes (Data from SI 2014)

Watershed		Soil Type	Constant head permeability test		Borehole shear test		
			Depth (m)	k (m/s)	Depth(m)	c (kPa)	ϕ (°)
Raemian	NB-1	Colluvium	1-2	4.67×10^{-6}	2.0	7.5	22.3
	NB-2	Colluvium	3-4	8.08×10^{-6}	2.0	6.9	25.1
		Weathered rock	5-6	1.99×10^{-6}	5.0	18.1	27.3
Deokuam	NB-3	Colluvium	1-2	8.08×10^{-6}	1.0	8.4	24.8
		Colluvium	3-4	1.02×10^{-6}	4.0	18.6	28.2
	NB-4	Colluvium	2-3	7.92×10^{-6}	2.0	11.9	27.0
		Weathered rock	8-9	9.55×10^{-7}	6.0	15.0	32.1
Hyongchon2	NB-5	Colluvium	1-2	3.54×10^{-6}	2.0	9.7	25.8
		Colluvium	4-5	2.24×10^{-6}	4.0	15.4	27.6
		Weathered rock	6-7	8.86×10^{-7}	7.0	32.7	31.3
	NB-6	Colluvium	1-2	4.45×10^{-6}	1.5	7.5	24.7
		Weathered rock	3-4	8.23×10^{-7}	3.0	33.8	32.6
	NB-7	Colluvium	1-2	2.08×10^{-6}			
		Colluvium	2-3	1.80×10^{-6}	5.0	11.2	27.1
		Weathered rock	5-6	8.30×10^{-7}			

Note: k is the permeability; c is the apparent cohesion; ϕ is the internal friction angle

Table 5. Geotechnical properties of the colluvial deposit from laboratory tests (Data from SI 2014)

Watershed		Depth (m)	w (%)	PL (%)	LL (%)	% Fines	USCS	c (kPa)	ϕ (°)
Raemian	TP-1	0.5	18.2	21.2	36.6	51.9	CL	9.2	21.7
	TP-2	0.5	14.1	22.3	31.6	28.9	SC	10.9	23.7
	TP-3	0.5	32.1	23.7	40.6	55.7	CL	11.3	23.1
	TP-4	0.5	15.8	20.9	35.9	44.4	SC	11.8	22.7
Deokuam	TP-5	0.15	21.2	23.0	41.6	55.1	CL	8.0	26.1
	TP-6	0.15	28.2	23.5	37.7	55.8	CL	10.6	27.2
Hyongchon2	TP-7	0.15	28.1	23.8	30.2	28.8	SM	6.6	32.1
	TP-8	0.15	30.6	23.0	42.1	54.2	CL	5.1	25.4

Note: w is the water content; PL is the plastic limit; LL is the liquid limit; % Fines<0.075 mm; USCS is the Unified Soil Classification System; c is the soil cohesion; ϕ is the soil friction angle

A conceptual methodology proposed for a typical susceptibility assessment of a shallow landslide based on a hydrological and geotechnical method is shown in Figure 16, and the YS-Slope was developed using this methodology. The YS-Slope uses unsaturated soil parameters such as field matric suction and SWCC. Various types of rainfall events like real-time rainfall and probability rainfall are used. Using the raster data with a matrix structure and the DEM, the rainfall infiltration depth and recharge into the groundwater considering the storage time were calculated for different times and locations of the watershed. It was used to calculate the safety factor at the second level. Finally, it can assess a rainfall-induced landslide depending on varying times using a groundwater table and wetting band depth.

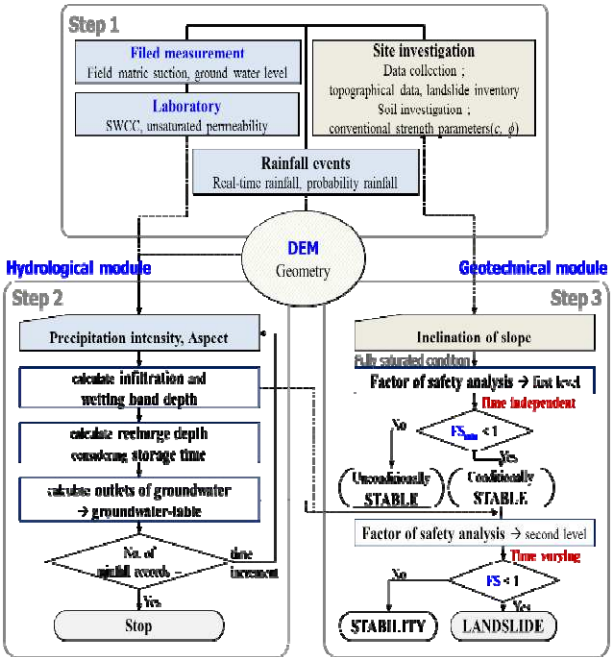

Figure 16. Flow chart of the proposed conceptual methodology

4.1.1 *Geotechnical infinite slope model*

Landslide analysis considers the infiltration by rainfall, which can be classified into three mechanisms: 1) a mechanism that considers the downward velocity of the wetting front, 2) a mechanism that considers the upward velocity of the groundwater level, and 3) a mechanism that considers both these factors. This model improves the infinite slope model for the first or second case to interpret the landslide susceptibility for the third mechanisms (Figure 17). The safety factor (FS) for the infinite slope is calculated from the ratio of the resisting stress on a slip surface to the gravitationally induced downward slope driving stress:

$$FS = \frac{(c_s' + c_r') + (\gamma_t \cdot D_s + q_0 + (\gamma_{sat} - \gamma_w) \cdot D_w) \cdot \cos^2\beta \cdot \tan\phi'}{(\gamma_t \cdot D_s + \gamma_{sat} \cdot D_w + q_0) \cdot \sin\beta \cdot \cos\beta} \quad (2)$$

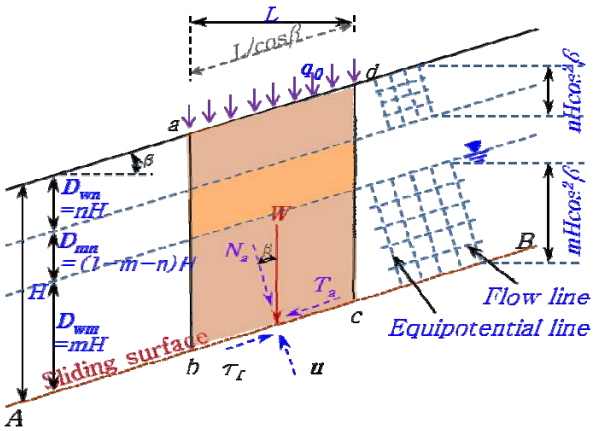

Figure 17. Infinite slippage plane for slope stability analysis, YS-Slope (Kim et al. 2014b)

4.1.2 *Hydrological model*

The hydrologic model is improved by incorporating the combined effects of groundwater flow and rain-fall infiltration into the raster model. This model was developed by considering the unsaturated soil behavior to estimate the rainfall-infiltration (I_R) and the recharge (R). The soil profile is ideally subdivided into three zones, i.e., the wetting band zone, partially saturated zone, and fully saturated zone, as shown in Figure 18. The vertical infiltration of water from the surface into the ground is modelled in the wetting band and partially saturated zones.

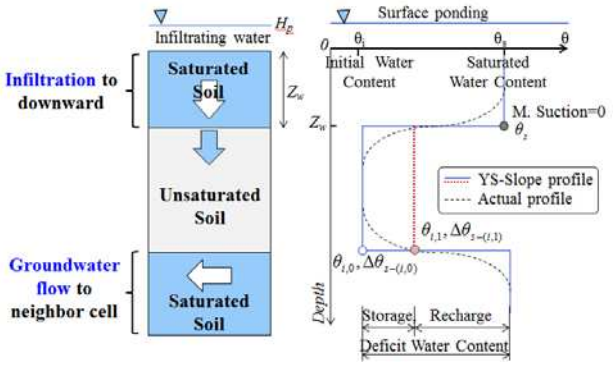

Figure 18. Typical soil profile and hydrologic model concept

The proposed model assumed that the volumetric water content and deficit water content remain constant above or below the wetting front. The groundwater flow was derived for

a small elemental volume, for which the properties of the soil were assumed to be effectively constant (Figure 19). A mass balance was done on the water flowing in and out of this small volume, and the flux was calculated in terms of the head using the constitutive equation of Darcy's law, which requires that the flow is slow.

The kinetic energy is neglected as described by Cedergren (1977). The total volume of the flow leaving the element (Q_x) in the x-direction for a unit time (Δt) can be expressed by assuming that the pore water pressure is constant over a small elementary volume of space. To apply the raster model, the total volume of flow leaving the element (Q_x) in a cell can be converted into the change in height (ΔH) using the deficit water content ($\Delta\theta$) and is expressed by

$$\Delta H_{ijk} = \frac{k_s \sin\beta_{ij} \; H_{ijk}}{s \; \Delta\theta} \; dt \qquad (3)$$

, where s is the distance between each cell, H_w is the height of groundwater in a cell (= dz), and θs is the volumetric water content. k is the permeability, i is hydraulic gradient, s is the distance through the soil, the subscript x (or y, z) denotes the x (or y, z)-direction, and $\sin\beta(= i = dh/ds)$ is the hydraulic gradient resulting from a difference in the groundwater potential across an element of the medium. The total volume of flow leaving the element and its flow direction were estimated using the eight-flow method (Jenson and Domingue, 1988). The flow of groundwater was calculated using the slope and slope direction of the bedrock. Based on the assumption that the kinetic energy is negligible, the total volume of flow leaving a cell can only be affected by the neighborhood cells. It is noted that a vector analysis including the watershed and drainage network is not required. Therefore, the flow of groundwater can be calculated from a cell to a neighborhood by shifting the change of the groundwater height based on equation (3).

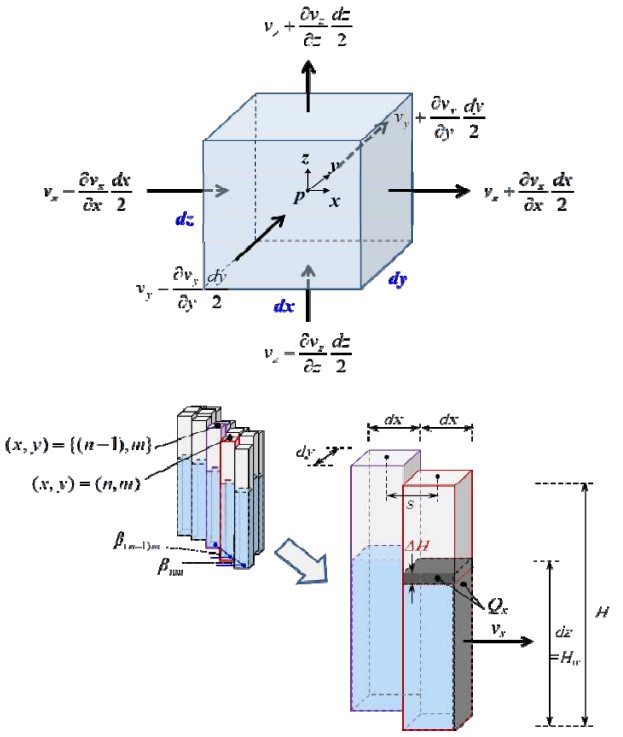

Figure 19. Fluid flow of an elementary volume of fluid in YS-Slope (Kim et al. 2014b)

4 .2 *Landslide susceptibility assessment*

4.2.1 *Experimental test*

To obtain the SWCC of the top soil on the Raemian watershed of Umyeonsan (Mt.), pressure plate extractor and filter paper tests were performed. The results of these tests are given in Figure 20. According to the Unified Soil Classification System (USCS), the top soil can be classified as SM (silty sand). The test results show a higher air-entry value, saturated- and residual-volumetric water contents.

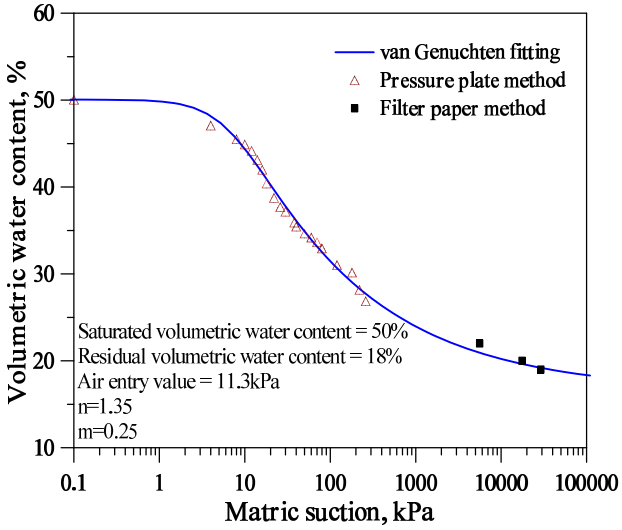

Figure 20. Soil-water characteristic curve (SI 2014)

Field matric suction was measured at the Raemian watershed from June 29 to July 19 in 2012. Three tensiometers depending on shallow- and middle- and deep-depths were installed, and then matric suctions were measured at the six different locations (T1-T6). Typically monitored results at T2 and T5 were selected and are shown in Figure 21. The initial matric suction measured at the site on June 29 before the rainy season was approximately 75 to 85 kPa. After the rainfall began, the matric suctions at 0.2 to 0.6 m depths rapidly decreased ranging from 0 to 16 kPa, and the matric suctions at 0.6 to 1.3 m gradually decreased to 20 kPa. At the depth of 1.4 m, the matric suction did not change during the six days because the infiltrated rainwater did not reach to this depth, whereas it tends to decrease after the 6th day. Since then, the matric suction in all tensiometers was maintained approximately at 10 to 20 kPa without further additional rainfall.

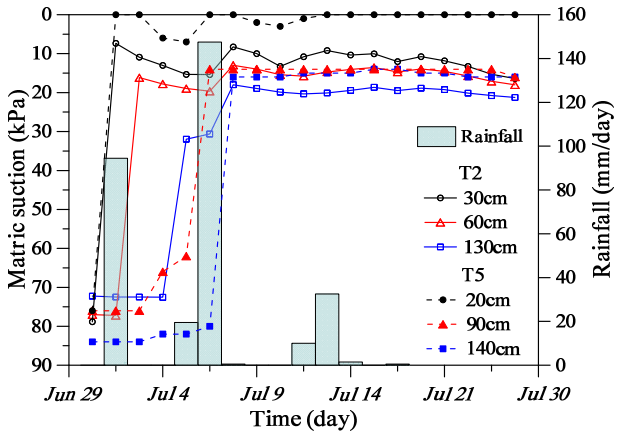

Figure 21. Measurement results and rainfall data (T2, T5) (SI 2014)

4.2.2 *Physically based GIS model*

A GIS-based landslide analysis was performed to determine the cause and failure mechanism using the proposed model. A 5×5 m gridded DEM converted from the 2009 LiDAR data, soil data obtained from detailed investigations and field measurements, and precipitation gauged by the auto weather station (AWS) of the KMA (2011) were used as the input data. A soil investigation was performed to obtain the detailed information of the soil properties, and is summarized in Table 2. Some soil properties (C_r' and q_o) were adopted from the literature (Clausnitzer et al. 1998, Norris 2008). To obtain a soil depth, a Krigging method was performed with the data from 14 bore-holes, a 2 km seismic prospecting, and a DEM (Figure 22).

Table 2. Geotechnical and hydraulic properties of the soil used in this study

Parameters	Values
Hydraulic conductivity, k_s	8×10^{-4} cm/s (28.8 mm/h)
Initial water contents, θ_i	28.0~32.0 (30.0) %
Water-content deficit, $\Delta\theta$	0.20
Soil cohesion, C_s'	10.2~12.8 (11.0) kPa
Soil friction angle, φ'	22.4~26.6 (26.5) °
Additional shear strength by roots of tree, C_r'	1.0 kPa
Uniform load by tree, q_0	0.253 kPa

Figure 23 shows the result of the landslide analysis using the proposed model in the Raemian and Limkwang1 and 2 watersheds. At the points of L3, L4 and L6 in the landslide inventory, it was assessed that the landslides occurred under the ground water table and at L1, L2 and L5 on the wetting front. Thus, two types of landslides occurred at this site, and a series of landslides were triggered by subsurface infiltration and the rising groundwater-table.

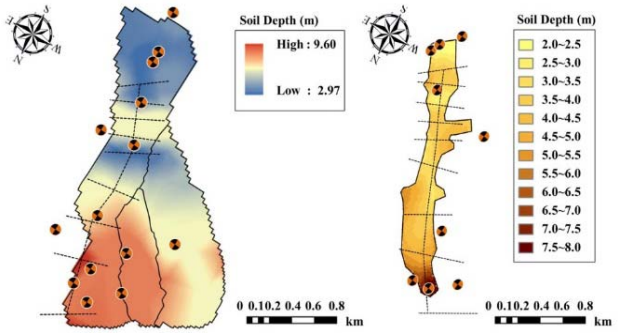

Figure 22. Map of the soil layer depth in Raemian (including Limkwang1, 2) and Dukuam watersheds (Kim et al. 2014b)

Figure 24 shows the result of the analysis using the predictive models in the Deokuam watershed. At this site, the results of the analysis for both mechanisms reasonably agree with all of the landslide observations. Because this site has generally a shallow soil depth of 2.0-3.0 m, it is sufficiently shallow in relation to the wetting band depth of 2.0 m at the site. Thus, this area was exposed to the same level of risk of landslide, which was triggered by subsurface infiltration and a rising groundwater-table. The results show the primary triggering factors causing landslides, i.e., soil depth and spatial and temporal distributions of groundwater variations.

Landslide source areas were collected by field surveys using a portable GPS, a laser ranger and a clinometer, which were 685 and 49 m^2 in the Raemian and Deokuam watersheds, respectively, and they were 0.53% of the total watershed area at test site 1 and 0.05% in the Deokuam watershed. These results of the field survey were compared with the numerical results obtained from the YS-Slope models (Table 3).

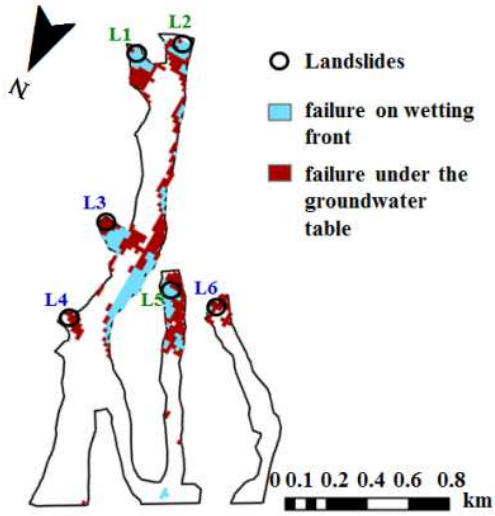

Figure 23. Type of slope failure in the Raemian and Limkwang1, 2 watersheds (Kim et al. 2014b)

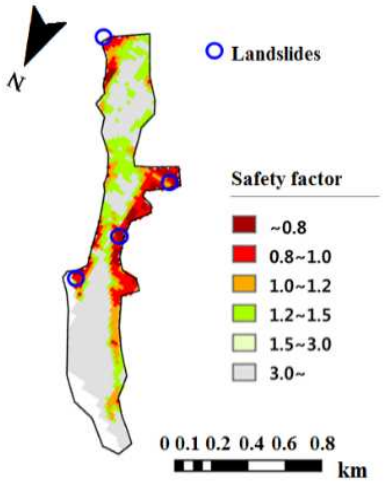

Figure 17. Slope failure in the case of Deokuam watershed (Kim et al. 2014b)

Table 3. Summary of landslide areas in the test sites

	Raemian		Dukwooam	
	Survey	YS-Slope	Survey	YS-Slope
Area (m^2)	685 (27)	4,672 (167)	49 (4)	2,013 (81)
% of area	0.53	3.63	0.05	2.04
Landslides	6	6	4	4
% landslides	-	100	-	100

( ) is number of unstable cell

5 CONCLUSIONS

In this paper, a comprehensive description of the landslide and debris flow hazards in Umyeonsan (Mt.) on July 27, 2011 was introduced with the morphological, hydrological, and geotechnical features of the watershed. Also, GIS-based

prediction methods were applied to assess the landslide susceptibility. The debris flow hazard resulted in 16 fatalities and extensive damage to houses, roads, and other properties. Most of the debris flows were initiated from shallow landslides which were triggered by an intensive rainstorm with a peak intensity of 112.5 mm/h. In total, 33 debris flows and 151 landslides occurred in 30 watersheds in the Umyeonsan area. Most of the landslides were concentrated along the ridgeline of the mountain due to the high slope angle. The slope material has a low density and low strength.

The physically-based GIS model for the simulation of the potential occurrences of shallow landslides on unsaturated soil by rainfall-infiltration, storage, recharge and groundwater flow processes was introduced and applied to two watersheds in Umyeonsan (Mt.). The analysis results showed that the all landslide locations from the field survey were included in the susceptible area by the proposed prediction model.

6 ACKNOWLEDGEMENTS

This research was supported by Public Welfare & Security R&D Program through the National Research Foundation of Korea (NRF) funded by the Ministry of Science, ICT and Future Planning (Grant No. 2012M3A2A1050979) and by Disaster Prevention Institute of Gangneung-Wonju National University.

7 REFERENCES

Cedergren H.R. 1977. *Seepage, drainage and flow nets*, New York.

Chen C.Y., Chen T.C., Yu F.C., Yu W.H. and Tseng C.C. 2005. Rainfall duration and debris-flow initiated studies for real-time monitoring. *Environ Geol* 47, 715–724.

Clausnitzer V. Hopmans J. and Starr J. 1998. Parameter uncertainty analysis of common infiltration models. *Soil Science Society of America Journal* 62. 1477-1487.

Coe J.A., Kinner D.A. and Godt J.W. 2008. Initiation conditions for debris flows generated by runoff at Chalk Cliffs, central Colorado. *Geomorphology* 96, 270–297.

Coussot P. and Meunier M. 1996. Recognition, classification and mechanical description of debris flows. *Earth Sci Rev* 40, 209–227.

Deganutti A.M., Marchi L. and Arattano M. 2000. Rainfall and debris-flow occurrence in the Moscardo basin (Italian Alps). *Proceedings of the second International Conference on Debris Flow Hazards Mitigation*, Taipei, Taiwan, 67–72.

Fleming R.W., Ellen S.D. and Algus M.A. 1989. Transformation of dilative and contractive landslide debris into debris flow-an example from Marin Country, California. *Eng Geol* 27, 201–223.

Fuchu D., Lee C.F. and Sijing W. 1999. Analysis of rainstorm-induced slide-debris flows on natural terrain of Lantau Island, Hong Kong. *Eng Geol* 51, 279–290.

Guzzetti F., Peruccacci S., Rossi M. and Stark C.P. 2008. The rainfall intensity-duration control of shallow landslides and debris flows: an update. *Landslides* 5, 3–17.

Hungr O., Leroueil S., and Picarelli L. 2014. The Varnes classification of landslide types, an update. *Landslides* 11 (2), 167-194.

Innes J.L. 1983. Debris flow. *Prog Phys Geogr* 7, 469–501.

Iverson R.M., Reid M.E., Logan M., LaHusen, R.G., Godt W.G. and Griswold, J.P. 2011. Positive feedback and momentum growth during debris flow entrainment of wet bed sediment. *Nature Geoscience* 4, 116-121.

Jenson S. and Domingue J. 1988. Extracting topographic structure from digital elevation data for geographic information system analysis. *Photogrammetric engineering and remote sensing* 54, 1593-1600.

Jeong S. Kim Y. Lee J.K. and Kim J. 2015. The 27 July 2011 debris flows at Umyeonsan, Seoul, Korea. *Landslides* 12 (4), 799-813.

KGS (Korean Geotechnical Society). 2011. *Final report on the cause of landslides in Umyeonsan(Mt.) area and the establishment of restoration measures*. Report No. KGS11-250 (In Korean)

Kim J. Jeong S. and Regueiro R.A. 2012. Instability of partially saturated soil slopes due to alteration of rainfall pattern. *Engineering Geology* 147–148, 28–36.

Kim H., Lee S.W., Yune C.Y. and Kim G. 2014a. Volume estimation of small scale debris flows based on observations of topographic changes using airborne LiDAR DEMs, *J. Mt. Sci.* 11 (3), 578-591.

Kim J., Lee K., Jeong S. and Kim G. 2014b. GIS-based prediction method of landslide susceptibility using a rainfall infiltration-groundwater flow model. *Engineering Geology* 182, 63-78.

Le T. and Bae D.H. 2013. Evaluating the utility of IPSS AR4 GCMs for hydrological application in South Korea. *Water Resour Manag* 27, 3227–3246.

Norris, J.E. 2008. *Slope stability and erosion control: ecotechnological solutions*. Springer.

SI (The Seoul Institute). 2014. *Final report on the cause of landslides in Umyeonsan(Mt.) - Complementary investigation*. Report No. 51-6110000-000649-01 (In Korean).

Soller D., Duncan I., Ellis G., Giglierano J. and Hess R. 1999. Proposed guidelines for inclusion of digital map products in the National Geologic Map Database. *Digital Mapping Techniques' 99 — Workshop Proceedings: US Geological Survey Open-File Report,* 99–386.

Son S.H., Choi B. and Paik J. 2012. Characteristics of rainfall and groundwater table in a small forested watershed of Mt. Umyeon. *Proceedings of 38th Korea Society of Civil Engineering Conference,* Gwangju, Korea. (In Korean)

Tiranti D., Bonetto S. and Mandrone G. 2008. Quantitative basin characterization to refine debris-flow triggering criteria and processes: an example from the Italian Western Alps. *Landslides* 5, 45–57.

Yune C.Y. Kim K.S. Yoo N.J., Seo H.S., and Jun K.J. 2011. Analysis of Debris Flow Characteristics through DATABASE Construction in Korea, *Italian Journal of Engineering Geology and Environment*, Special Volume, 159-164.

Yune C.Y. Chae, Y.K. Paik J. Kim, G. Lee S.W. and Seo H.S. 2013. Debris Flow in Metropolitan Area - 2011 Seoul Debris Flow, *J. Mt. Sci.* 10 (2), 199-206.

Zhou W., Tang C., Asch T.W.J.V. and Zhou C. 2014. Rainfall-triggering response patterns of post-seismic debris flow in the Wenchuan earthquake area. *Nat Hazards* 70, 1417–1435.